

Fast, sensitive and spectrally tuneable colloidal-quantum-dot photodetectors

Jason P. Clifford, Gerasimos Konstantatos, Keith W. Johnston, Sjoerd Hoogland, Larissa Levina and Edward H. Sargent*

Solution-processed semiconductors are compatible with a range of substrates, which enables their direct integration with organic circuits^{1,2}, microfluidics^{3,4}, optical circuitry^{1,5} and commercial microelectronics. Ultrasensitive photodetectors based on solution-process colloidal quantum dots operating in both the visible and infrared have been demonstrated^{6,7}, but these devices have poor response times (on the scale of seconds) to changes in illumination, and rapid-response devices based on a photodiode architecture suffer from low sensitivity⁸. Here, we show that the temporal response of these devices is determined by two components—electron drift, which is a fast process, and electron diffusion, which is a slow process. By building devices that exclude the diffusion component, we are able to demonstrate a >1,000-fold improvement in the sensitivity-bandwidth product of tuneable colloidal-quantum-dot photodiodes operating in the visible and infrared^{6–8}.

Colloidal quantum dots (CQDs) combine quantum size effect tuning with the practical advantages of solution processing. Quantum size effect tuning allows the energy bandgap and absorption onset of CQDs to be varied over a wide range of wavelengths in the visible and infrared (IR)⁹. Operation at IR wavelengths allows the detection of light transmitted through atmospheric¹⁰, biological^{11,12} and other materials absorption windows, dramatically increasing the range of potential applications. The ability to limit spectral absorption is also important for photodetector applications; the bandgap should only be as small as is necessary to absorb photons of interest, while rejecting background photons and minimizing internal noise that would otherwise limit sensitivity.

Photoconductive CQD photodetectors have recently been reported with remarkable sensitivities up to 1×10^{13} Jones (refs 7, 8) (see Supplementary Information, Section 1, for a definition of photodetector sensitivity). As a result, slow modulation response and narrow response bandwidth (<20 Hz) have been tolerated in these devices, but these limitations severely curtail potential applications.

An alternative photodetector architecture, the photodiode, offers the potential of significantly higher response speed. However, the only report of a fast CQD detector (50 kHz bandwidth) demonstrated a sensitivity of approximately 1×10^7 Jones (ref. 8)—five orders of magnitude lower than crystalline semiconductor photodetectors.

In this work, we took the view that reliance on the long-lived minority carrier traps essential to photoconduction would necessarily lead to slow response speeds. We therefore pursued the charge-separating photodiode architecture, recognizing that an orders-of-magnitude improvement in sensitivity would be required.

CQD films offer a number of chemically tuneable degrees of freedom that provide control over their macroscopic electronic properties. The spacing between individual CQDs is controlled by

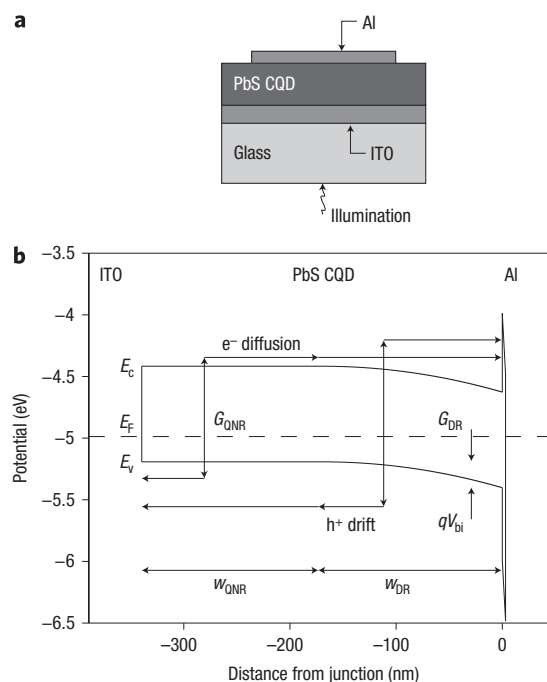


Figure 1 | Photodiode structure, energy bands and photocurrent components.

a, A schematic representation of the photodiode device architecture. **b**, The Schottky barrier at the Al/PbS (Q1) interface forms a depletion region in the CQD film with a bias-dependent width (w_{DR}) and a built-in potential (V_{bi}). The remaining width of the CQD film (w_{QNR}) is unaffected by the Schottky barrier and is designated as a quasi-neutral region. Electrons and holes generated in the depletion region (G_{DR}) drift under the influence of the electric field to the aluminium contact and the edge of the quasi-neutral region, respectively. Electrons generated in the quasi-neutral region (G_{QNR}) must diffuse to the edge of the depletion region, where they are rapidly swept away by the electric field. The movement of holes in the quasi-neutral region is governed by the relaxation of the p-type semiconductor.

the length of the organic ligands used to passivate their surfaces and has been shown to be a determining factor in the charge carrier mobility and conductivity of CQD films^{8,13,14}. The consistency of surface passivation is also important, as this limits oxidation and other chemical modification of the CQD surface. Oxidation provides a route to dope CQD films^{14,15}, however, uncontrolled variation in the CQD surface leads to interface states and a reduction of the built-in potential when forming metallurgical junctions.

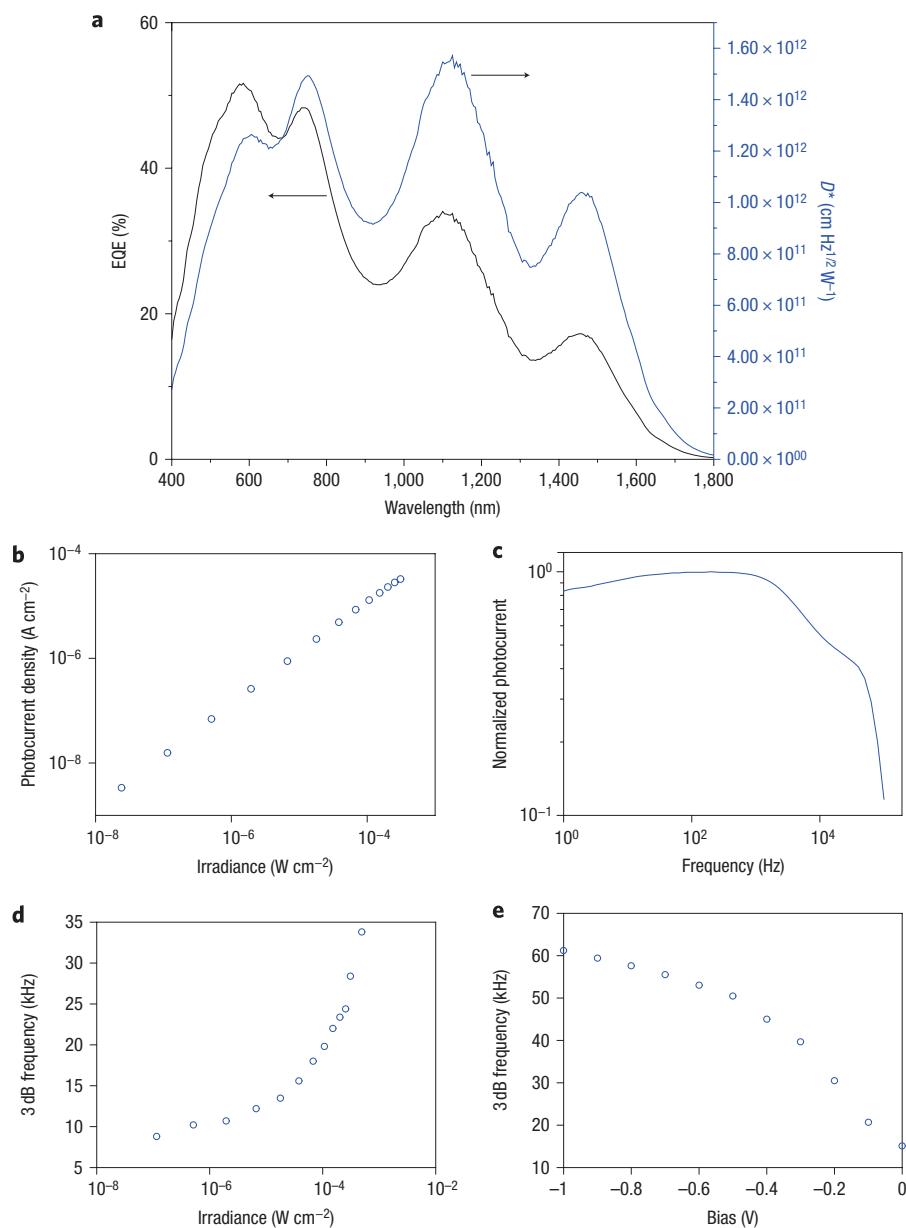


Figure 2 | Photodiode spectral response, illumination response and frequency response. **a**, External quantum efficiency (at 295 K) and normalized detectivity (at 250 K) as a function of wavelength. **b**, Photocurrent density as a function of irradiance at 1,550 nm. **c**, Frequency dependence of photocurrent at zero bias and $17.9 \mu\text{W cm}^{-2}$ irradiance at 1,550 nm. **d**, Frequency dependence (3 dB) on irradiance. **e**, Frequency dependence (3 dB) on bias.

In diodes, the energetic barrier associated with the metallurgical junction defines the effective shunt resistance (R_{sh}), which, in turn, determines noise performance.

We fabricated photodiodes based on a Schottky barrier at the interface between a PbS CQD film and an aluminium contact (Fig. 1a). A planar, transparent indium tin oxide (ITO) thin film formed the opposing ohmic contact. Light incident through the glass substrate generates electrons and holes in the CQD film that are collected at the aluminium and ITO contacts, respectively. The energy band diagram in Fig. 1b shows the Schottky barrier formed at the Al/PbS CQD interface¹⁶, and the built-in potential derived from the difference in work function between the CQDs and the metal contact. A depletion region in the CQD film forms at the metal–CQD interface, whereas the remaining volume of CQD film is a quasi-neutral region of p-type semiconductor¹⁶. The large potential barrier in the valence band limits majority

carrier (hole) injection from the aluminium contact, resulting in highly rectifying dark I – V characteristics¹⁶.

We synthesized PbS CQDs with a diameter of ~ 6 nm, increasing the effective bandgap from the bulk PbS value of 0.42 eV to 0.86 eV through the quantum size effect⁹. This effective bandgap corresponds to a ground-state excitonic absorption feature at 1,450 nm.

A three-stage CQD surface modification strategy was used to create films of densely packed CQDs with stable benzenedithiol (BDT) surface passivation and controlled effective doping (see Supplementary Information, Section 2). BDT treatment of the CQD films increased photodiode lifetime from ~ 4 h to >2 months and dramatically reduced short-circuit dark current densities from ~ 100 to below 0.1 nA cm^{-2} . The 1,000-fold decrease in short-circuit dark current is attributed to the elimination of primary butylamine ligands in the CQD film and their interaction with the aluminium contact. The noise associated with this

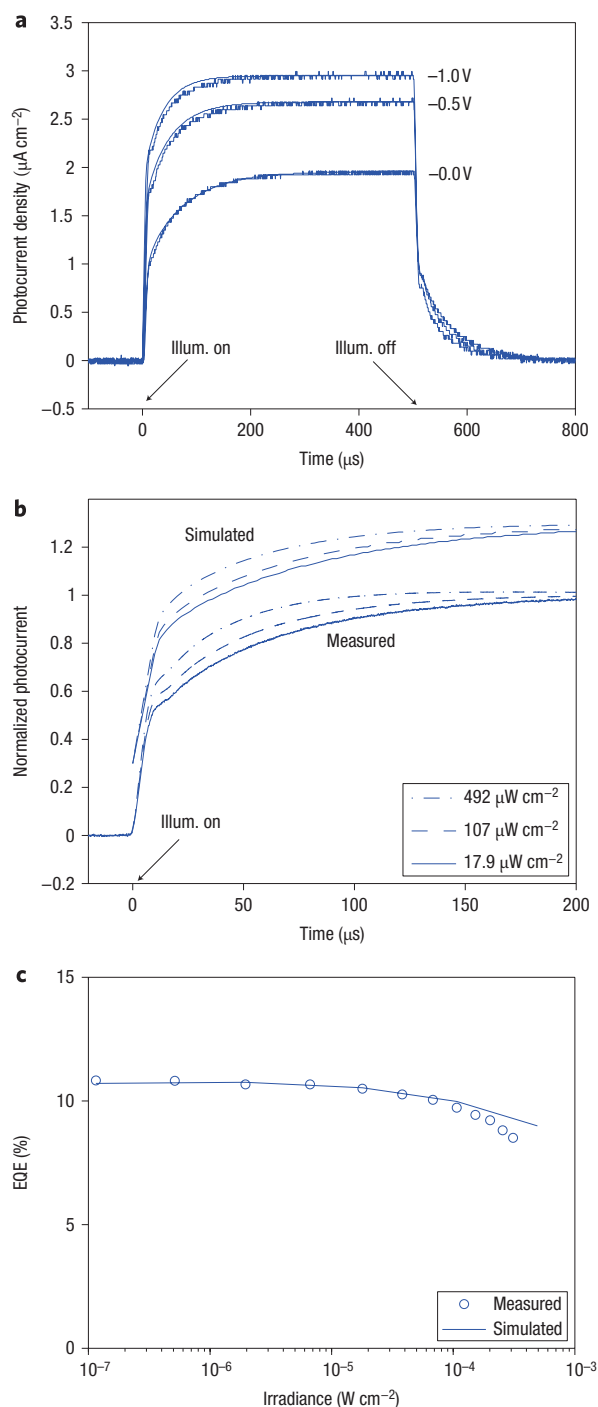


Figure 3 | Photodiode transient response and quantum efficiency as a function of bias and irradiance. **a**, Measured (noisy line) and simulated (smooth line) photocurrent transient response, as a function of bias, to a 500- μs -square illumination pulse at 17.9 $\mu\text{W cm}^{-2}$ at 1,550 nm. Note that the measured and simulated lines are co-incident for 0.0 V. **b**, Measured and simulated photocurrent transient response (normalized) as a function of irradiance at zero bias. The simulated response is shifted for clarity. **c**, Measured and simulated EQE as a function of irradiance at 1,550 nm.

electrochemical dark current previously limited the detectivity of CQD photodiodes to $\sim 1 \times 10^{10}$ Jones.

Figure 2a shows external quantum efficiency (EQE) (at 295 K) and normalized detectivity (at 250 K) as a function of wavelength in the CQD photodiode. The shape of the EQE and D^* spectra

follows the absorption spectrum of the CQD film (see Supplementary Information, Section 3). The peak in the absorption and EQE at 1,450 nm corresponds to the ground-state CQD excitonic absorption feature, whereas peaks in EQE at shorter wavelengths are the result of Fabry–Perot interference in the thin CQD film. Figure 2b shows photocurrent density as a function of irradiance. The photoresponse is linear within 6% over 4 decades of irradiance. (See Supplementary Information, Section 4, for current–voltage characteristics of the photodetector.)

The dramatic increase in EQE compared to previous CQD photodiode photodetectors was achieved by creating a large (0.20 V) built-in potential for photogenerated charge carrier separation. Controlled oxidization increased the doping of the CQD film (after treatment with a reducing agent, BDT) and the height of the Schottky barrier at the Al/PbS CQD metallurgical junction. The optimal duration of the oxidation process was determined empirically to provide the largest built-in potential before growth of interfacial states at the metallurgical junction began to degrade EQE.

Figure 2c shows normalized photocurrent in the photodiode as a function of illumination modulation frequency. The poles (onset of an exponential decay in response) at 1 and 50 kHz correspond to the time required to reach the steady state in the quasi-neutral region and the transit time of the depletion region, ~ 500 and ~ 10 μs , respectively, as shown in Fig. 3a,b and discussed below. Figure 2d,e shows an exponential dependence of the 3 dB frequency on irradiance and a sublinear dependence of the 3 dB frequency on reverse bias.

Under zero-bias conditions and in the absence of illumination, noise current in photodiodes is proportional to R_0A , the product of the zero-bias effective shunt resistance and the device area. In the CQD photodiode, R_0A increases with decreasing temperature from $1 \times 10^5 \Omega \text{ cm}^2$ at 300 K to just under $1 \times 10^7 \Omega \text{ cm}^2$ at 235 K (see Supplementary Information, Section 5)—values comparable to highly optimized crystalline semiconductor photodiodes.

The magnitude of R_0A (and the dark short-circuit current) is typically dependent on the bandgap of the semiconductor, as a larger bandgap enables a larger Schottky barrier. We maximized R_0A through effective CQD surface passivation, which limits surface states at the Al/PbS CQD metallurgical junction. Despite working with an IR-sensitive semiconductor, we achieved a 1,000-fold reduction in short-circuit noise current and a 100-fold reduction in short-circuit dark current compared to recent reports on visible CQD photodetectors based on wider bandgap semiconductors⁸.

The speed and sensitivity of the CQD photodiode represents a 3,300-fold improvement in response speed and an 11 orders-of-magnitude reduction in dark current density over the most sensitive CQD photodetector reported⁶. D^* values of 1×10^{12} Jones represent sensitivity on the order of commercially available photodetectors fabricated with crystalline semiconductors such as silicon and InGaAs. Equally important, this represents a 100,000-fold improvement in sensitivity and response speeds up to 20% greater than the fastest CQD photodetector reported⁸.

We used the transient response to stepwise changes in illumination, combined with a physical model, to establish the operation of the CQD photodiode. Figure 3a shows the photocurrent response to a 500- μs -square illumination pulse at biases of 0.0, -0.5 and -1.0 V. At each bias, the transient response is composed of two components: an initial, fast, linearly increasing component, and a slower component that exponentially settles to a steady state. The rise-and-fall characteristics of the photocurrent are symmetric. The fast component is attributed to carriers generated in the depletion region (G_{DR} in Fig. 1b) and swept out as a drift current proportional to the built-in electric field (E). The rise time of this component is the time required to transit the depletion region ($t_{\text{tr}} = w_{\text{DR}}/[\mu_{\text{drift}}E]$), where μ_{drift} is

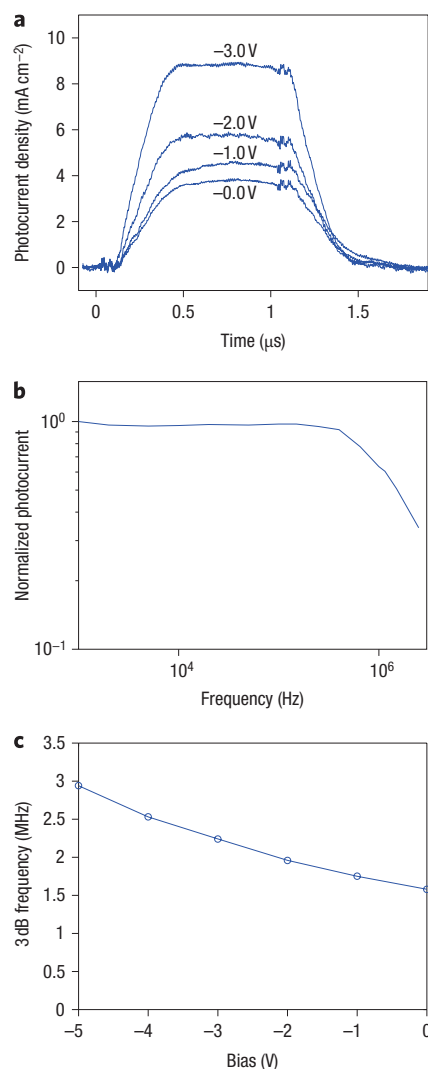


Figure 4 | Fully depleted photodiode spectral response and frequency response. **a**, Photocurrent transient response, as a function of bias, to a 1- μ s-square illumination pulse at 40 mW cm^{-2} and 1,550 nm. **b**, Frequency dependence of photocurrent at zero bias and 40 mW cm^{-2} irradiance at 1,550 nm. **c**, Frequency dependence (3 dB) on bias.

the drift mobility, approximately the same for both electrons and holes according to measured drift mobilities (see Supplementary Information, Section 9). The slower component is attributed to electrons generated in the quasi-neutral region (G_{QNR} in Fig. 1b) that must diffuse to the depletion region. The rise time of this component is the time required for generation, diffusion and recombination in the quasi-neutral region to reach a steady state, and is dependent on the width of the quasi-neutral region (w_{QNR}) and inversely dependent on the electron diffusivity (D_e). Measurement of photodiodes fabricated from polydispersed CQD films indicated that exciton diffusion does not play a significant role in photodiode operation (see Supplementary Information, Section 6).

We have developed a numerical model that solves the continuity equations for electrons and holes in the quasi-neutral and depleted regions of the CQD photodiode based on measured materials and device parameters (see Supplementary Information, Sections 7 to 11). The model accurately depicts the dependence of the photocurrent transient on bias and irradiance, as shown in Fig. 3a,b. Using the measured carrier lifetime dependence on

irradiance, the numerical model also quantitatively predicts the dependence of photodiode EQE on irradiance, as shown in Fig. 3c. Photodiode EQE is independent of irradiance at irradiances $< 1 \times 10^{-5} \text{ W cm}^{-2}$, but begins to decrease at irradiances $> 1 \times 10^{-5} \text{ W cm}^{-2}$. This transition corresponds to the minimum carrier lifetime required for photocarriers generated in the quasi-neutral region to diffuse to the edge of the depletion region.

The EQE of CQD photodiodes is determined by three processes, each characterized by an efficiency ranging from 0 to 1:

$$\eta_{\text{external}} = \eta_{\text{abs}} \cdot \eta_{\text{diss}} \cdot \eta_{\text{extr}}$$

η_{abs} is the fraction of the incident photon flux absorbed by the CQD film, η_{diss} represents the probability of photogenerated excitons dissociating into individual charge carriers, and η_{extr} quantifies the efficiency with which these charge carriers are transported, through drift and diffusion, to the contacts. We determined η_{abs} to be $\sim 37\%$ at the excitonic absorption feature (1,450 nm). η_{extr} approaches unity below irradiances of $1 \times 10^{-5} \text{ W cm}^{-2}$, because the drift length and diffusion lengths exceed the depletion region and quasi-neutral region depths, respectively (see Supplementary Information, Section 12). η_{diss} therefore lies in the range 40–60%, depending on bias, to account for the observed external EQE of 17 to 25% at 1,450 nm over the bias range 0.0 to -1.0 V.

The model of CQD photodiode operation pointed to a clear conclusion: an efficient and much faster CQD photodiode could be developed if photocarriers could be transported by drift alone. By reducing the thickness of the CQD film to equal the width of the depletion region (180 nm), we fabricated a fully depleted photodiode in which all photogenerated electrons and holes are swept directly to the contacts by the electric field resulting from the built-in potential of the junction and any externally applied bias. Figure 4a shows that transient photocurrent response to a 1- μ s-square illumination pulse is indeed limited only by the drift transit time (~ 300 ns).

The drift transit time of the CQD photodiode was further reduced by increasing the mobility of the CQD film through a more complete ligand exchange than that used in the initial CQD photodiode development (majority carrier hole mobility increased from 1×10^{-4} to $6 \times 10^{-4} \text{ cm}^2 \text{ V}^{-1} \text{ s}^{-1}$). The frequency response of the fully depleted photodiode is shown in Fig. 4b. The 3 dB frequency increases with reverse bias, as shown in Fig. 4c, due to a reduction in carrier transit time with increasing electric field in the depletion region. The device remains linear within 10% over six decades of irradiance. The short-circuit dark current density was unchanged from the previous device at $< 0.1 \text{ nA cm}^{-2}$.

The response speed of the fully depleted CQD photodiode represents a significant improvement over all reported CQD photodetectors: a 170,000-fold improvement in response speed over the most sensitive CQD photodetector reported⁶, and a 60-fold improvement in response speed over the fastest CQD photodetector reported⁸. With $D^* > 1 \times 10^{11}$ Jones at room temperature, this device maintains a 10,000-fold improvement in sensitivity over the fastest CQD photodetector reported⁸.

The combination of speed and sensitivity demonstrated by the fully depleted CQD photodiode represents a $> 1,000$ -fold improvement in sensitivity–bandwidth product relative to all previous CQD photodetectors. This improvement in device performance was achieved by designing a photodiode architecture to take advantage of insights into charge carrier transport and by tailoring the CQD film passivation to support both high carrier mobilities and a large built-in potential at a metallurgical junction.

Methods

PbS CQD synthesis and ligand exchange. PbS CQDs with an excitonic peak at $\sim 1,500$ nm were prepared by injection of 2.0 mmol bis(trimethylsilyl)sulphide) into

a reaction flask containing 4.0 mmol lead oxide (0.9 g), 9.5 mmol oleic acid (2.67 g) and 18.8 mmol octadecene (4.73 g) at 120 °C. After injection, the reaction was quenched by moving the flask to an ice-water bath.

The synthesis was carried out under inert conditions using a Schlenk line. The final PbS oleate-capped CQDs were isolated from any remaining starting materials and side products by precipitating with acetone and re-dissolving in toluene, repeated twice.

Solution-phase ligand exchange required precipitating the CQDs with methanol and redissolving in toluene twice before a final precipitation with methanol and redissolving in primary butylamine. The mixture was left for 3 days at room temperature, then precipitated with isopropanol and redispersed in octane. All processing was carried out in a glove box with an N₂ atmosphere.

Films (350-nm-thick) were formed by spin-coating CQDs suspended in octane onto commercial glass substrates coated with conductive ITO. After film deposition, the CQDs were treated in a 5 mg ml⁻¹ solution of BDT in acetonitrile for up to 60 min. Aluminium contacts (100 nm thick, 1.96 mm² area) were deposited on top of this film by thermal evaporation at $\sim 1 \times 10^{-5}$ torr. The complete devices were subsequently exposed to a high-humidity air atmosphere at 35 °C for up to 12 h to accelerate oxidation of the CQD film. CQD film deposition was carried out in an inert environment, and BDT treatment and subsequent handling was performed under ambient conditions.

Monochromatic photoresponse. Devices were illuminated through the glass substrate and ITO transparent contact. Uniform illumination was provided by a Roithner Lasertechnik 1,550 nm LED array with an Agilent 33220A 20 MHz function generator used to supply a constant or modulated bias to the LEDs. The irradiance was calibrated using a Newport 2930C power meter and 918-IG calibrated photodetector placed at the position of the CQD photodiode. Steady-state current was measured with a Keithley 6430 sub-femtoamp SourceMeter and transient currents were measured with a Stanford Research SR570 low-noise current preamplifier and a Tektronix TDS 220 or TDS 5104 digital oscilloscope. Biases, if used, were supplied by the SourceMeter or current preamplifier. Frequency, wavelength and illumination dependencies of the photocurrent were measured with a Stanford Research SR830 lock-in amplifier in current measurement mode. All measurements were performed in a dark, shielded enclosure at room temperature (295 K) in air, except for the temperature-controlled measurements, which were measured in an N₂ atmosphere using a liquid nitrogen bath cryostat.

High-speed characterization of the fully depleted CQD photodiode used a JDS Uniphase SWS15101 Tunable Laser Source modulated by an Agilent 33220A 20 MHz function generator. The rise and fall time of the laser were measured at 40 and 60 ns, respectively. Photocurrent was measured using a 25 Ω resistive load as a transimpedance stage and a Tektronix TDS 5104 digital oscilloscope. High illumination intensities (40 mW cm⁻²) were used to provide suitable signal-to-noise ratios for measurements.

Spectral photoresponse. Monochromatic illumination was provided by a Jobin Yvon Triax 320 monochromator with a ScienceTech TH-PS white light source. Multimode optical fibres were used to direct the light to a collimator and the CQD photodiode. Incident irradiance was invariant within 4% from 400 to 1,800 nm. The light was mechanically chopped at 100 Hz and the photocurrent response at zero bias was recorded with a Stanford Research SR830 lock-in amplifier. The spectral photocurrent was scaled to match the monochromatic response measured at 1,550 nm. All measurements were performed in a dark, shielded enclosure at room temperature.

Noise. Noise was measured in the dark, at zero bias, using a Stanford Research SR830 Lock-in Amplifier in current measurement mode. Noise current was measured directly using the lock-in amplifier and normalized by the input bandwidth. All measurements were performed in a dark, shielded enclosure at room temperature (295 K) in air, except for the temperature-controlled measurements which were measured in an N₂ atmosphere using a liquid nitrogen bath cryostat.

Dark short-circuit current. Steady-state current under dark conditions was measured with a Keithley 6430 sub-femtoamp SourceMeter. Dark current under short-circuit conditions was below a measurable limit of 0.1 nA cm⁻² determined by

the voltage overburden of the instrumentation (20 μV) and the effective shunt resistance of the photodiode (8 MΩ).

Received 1 August 2008; accepted 24 September 2008;
published 9 November 2008

References

- Xue, J. & Forrest, S. R. Organic optical bistable switch. *Appl. Phys. Lett.* **82**, 136–138 (2003).
- Kymissis, I., Sodini, C. G., Akinwande, A. I. & Bulovic, V. An organic semiconductor based process for photodetecting applications. *2004 IEDM Tech. Dig.*, 377–380 (2004).
- Hofmann, O. *et al.* Thin-film organic photodiodes as integrated detectors for microscale chemiluminescence assays. *Sens. Actuators B* **106**, 878–884 (2005).
- Wang, X. Integrated thin-film polymer/fullerene photodetectors for on-chip microfluidic chemiluminescence detection. *Lab. Chip* **7**, 58–63 (2007).
- Morimune, T., Kajii, H. & Ohmori, Y. Semitransparent organic photodetectors utilizing sputter-deposited indium tin oxide for top contact electrode. *Jpn J. Appl. Phys.* **44**, 2815–2817 (2005).
- Konstantatos, G. *et al.* Ultrasensitive solution-cast quantum dot photodetectors. *Nature* **442**, 180–183 (2006).
- Konstantatos, G., Clifford, J. P., Levina, L. & Sargent, E. H. Sensitive solution-processed visible-wavelength photodetectors. *Nature Photon.* **1**, 531–534 (2007).
- Oertel, D. C., Bawendi, M. G., Arango, A. C. & Bulovic, V. Photodetectors based on treated CdSe quantum-dot films. *Appl. Phys. Lett.* **87**, 2135051 (2005).
- Wise, F. W. Lead salt quantum dots: the limit of strong quantum confinement. *Acc. Chem. Res.* **33**, 773–780 (2000).
- Jones, A. V. The infrared spectrum of the airglow. *Space Science Rev.* **15**, 355–400 (1973).
- Sargent, E. H. Infrared quantum dots. *Adv. Mater.* **17**, 515–522 (2005).
- Kim, S. *et al.* Near-infrared fluorescent type II quantum dots for sentinel lymph node mapping. *Nature Biotechnol.* **22**, 93–97 (2004).
- Jaros, M. V., Porter, V. J., Fisher, B. R., Kastner, M. A. & Bawendi, M. G. Photoconductivity studies of treated CdSe quantum dot films exhibiting increased exciton ionization efficiency. *Phys. Rev. B* **70**, 195327 (2004).
- Luther, J. M. *et al.* Structural, optical and electrical properties of self-assembled films of PbSe nanocrystals treated with 1,2-ethanedithiol. *ACS Nano* **2**, 271–280 (2008).
- Talapin, D. V. & Murray, C. B. PbSe nanocrystal solids for n- and p-channel thin film field-effect transistors. *Science* **310**, 86–89 (2005).
- Clifford, J. P., Johnston, K. W., Levina, L. & Sargent, E. H. Schottky barriers to colloidal quantum dot films. *Appl. Phys. Lett.* **91**, 2531171 (2007).

Acknowledgements

The authors thank D. Grozea for performing the XPS measurements.

Author contributions

J.P.C. conceived and fabricated the CQD photodiodes, performed all device performance characterization, and conceived and implemented the CQD photodiode device model. G.K. coordinated and interpreted the XPS measurements. K.W.J. and J.P.C. co-developed the first step of the CQD surface modification strategy. S.H. and J.P.C. co-developed the second step of the CQD surface modification strategy. L.L. synthesized all CQDs used to fabricate the devices. E.H.S. assisted in interpretation of the results, commented on the device model, and commented on the manuscript. All authors discussed the results and the capacity of the model to describe the underlying physics of device operation.

Additional information

Supplementary Information accompanies this paper at www.nature.com/naturenanotechnology. Reprints and permission information is available online at <http://npg.nature.com/reprintsandpermissions/>. Correspondence and requests for materials should be addressed to E.H.S.